A Reappraisal of the Thermal Growing Season Length across Europe

Richard C. Cornes[1,2*], Gerard van der Schrier[1], and Antonello A. Squintu[1]

[1] *Royal Netherlands Meteorological Institute (KNMI), De Bilt, Netherlands*
[2] *Current affiliation: National Oceanography Centre, Southampton, UK*
[*] *Corresponding author: richard.cornes@noc.ac.uk*

Abstract

Growing Season Length (GSL) indices derived from surface air temperature are frequently used in climate monitoring applications. The widely used Expert Team on Climate Change Detection and Indices (ETCCDI) definition aims to give a broadly-applicable measure of the GSL that is indicative of the duration of the mild part of the year. In this paper long-term trends in that index are compared with an alternative measure calculated using a time-series decomposition technique (Empirical Ensemble Mode Decomposition [EEMD]). It is demonstrated that the ETCCDI index departs from the mild-season definition as its start and end dates are determined by temperature events operating within the synoptic timescale; this raises the interannual variance of the index. The EEMD-derived index provides a less noisy and more realistic index of the GSL by filtering out the synoptic-scale variance and capturing the annual-cycle and longer timescale variability. Long-term trends in the GSL are comparable between the two indices, with an average increase in length of around 5 days decade^{-1} observed for the period 1965–2016. However, the results using the EEMD index display a more coherent picture of significant trends than has been previously observed. Furthermore, the EEMD-derived growing season parameters are more closely related to variations in seasonal-mean hemispheric-scale atmospheric circulation patterns, with around 57% of the interannual variation in the start of the growing season being connected to the North Atlantic Oscillation and East Atlantic patterns, and around 55% of variation in the end of the growing season being associated with East Atlantic/West Russia-type patterns.

Keywords: EEMD, ETCCDI, Synoptic variability, Temperature trends

Short Title: The Thermal Growing Season Length across Europe

1 Introduction

The thermal growing season length (GSL) is a measure derived from surface air temperature data and is widely used in climate monitoring to indicate the length of time that vegetation growth is theoretically possible for a given year. Numerous definitions of the GSL exist, and these often necessarily vary depending on the region under consideration (Linderholm, 2006). A common way of defining the GSL is to calculate the length of time between the first and last frost of the year, where frost is determined from daily minimum air temperatures at or below 0°C (e.g. Robeson, 2002; Kunkel et al., 2004; Yu et al., 2014; Strong and McCabe, 2017; Wypych et al., 2017). Although the frost-free period has relevance for certain regions and for many types of vegetation, a more broadly applicable definition — particularly for mid- to high-latitude areas (Walther and Linderholm, 2006) — is used by the Expert Team on Climate Change Detection and Indices (ETCCDI). In the Northern Hemisphere the ETCCDI define the GSL for a given year (1st Jan to 31st Dec) as the number of days between the first span of at least six days when daily mean temperature is greater than 5°C and the first span after 1st July when temperature is below 5°C. In the southern hemisphere the year runs from 1st July to 30th June of the following year (Zhang et al., 2011).

The span of six consecutive days is used in the ETCCDI GSL definition to reduce the effect of high-frequency, weather-related variability on the index. As such the index is intended to provide a measure of the duration of the mild part of the year with the start and end dates loosely indicative of general phenological phase-changes (Zhang et al., 2011). However, the index remains susceptible to weather-related variance because the start and end dates are determined from synoptic-scale temperature events that are typically operating on timescales of up to around 11 days. This is potentially one reason behind the observation that growing season (GS) statistics tend to be very noisy on an interannual basis (Robeson, 2002).

The susceptibility of the ETCCDI GSL index to synoptic-scale variability is demonstrated in Figure 1 where the GSL has been calculated for the year 2013 using the daily Central England Temperature (CET) series (Parker et al., 1992). March 2013 was particularly cold across England, with persistent, easterly winds and frequent falls of snow experienced; it was the coldest March since 1962 (Eden, 2013). However, for 2013 the ETCCDI GSL index starts on 1st January, due to a week of mild temperatures at the start of the year, and ends on the 31st December, due to an absence of consecutive days above the 5°C threshold after 1st July. Hence the GSL for 2013 was 365 days, despite a significant delay to agriculture being widely reported; a similar, although less extreme, situation occurred in January 2018. These are typical examples of false-springs (Davis, 1972) and the use of a refined GSL index that takes into account the occurrence of frost, along with the 5°C criterion, may provide a more realistic index of GS onset (Jones et al., 2002; Walther and Linderholm, 2006). However, as demonstrated in Figure 1, a better index of the GSL could be developed using a time-series decomposition technique such as Empirical Ensemble Mode Decomposition (EEMD), which filters the higher-frequency, weather variability from the lower frequency annual cycle. This way of calculating the GSL was proposed by Qian et al. (2009), who used the technique to calculate the timing of spring onset in the long Stockholm temperature series. In this paper we examine trends and variability in the thermal GSL across Europe by comparing the ETCCDI index against an EEMD-derived metric. The EEMD method is particularly suitable for this type of calculation since the low-frequency annual cycle and longer-term component (ALC) are captured using a temporally local and adaptive low-pass filter (Qian et al., 2011b).

2 Defining the Growing Season Length

2.1 Datasets

The daily mean, blended temperature series from the ECA&D database (Klein Tank et al., 2002; Klok and Klein Tank, 2009) are used in this paper. The data have been homogenized using the method described by Squintu et al. (2018). Since there are relatively few stations that extend earlier than 1950 in the database, the analysis is restricted to the period 1965–2016. To provide a longer context we also calculate the GSL parameters from three multi-centenary time series: the daily Central England Temperature (CET) series (which covers the period 1772–2017, Parker et al., 1992), the Stockholm temperature series (1722–2017, Moberg et al., 2002) and the St Petersburg temperature series (1805–2017, Jones and Lister, 2002). The latter series has been extended to 2017 from the original 1999 cutoff using data for St Petersburg contained in the ECA&D database. Although the series stretches back to 1743, there are too many missing values in the early part of the series to compute the indices before 1805.

2.2 The EEMD method

EEMD is a time-series decomposition technique that extracts a set of oscillation components from a time series (Wu and Huang, 2009). These components are termed Intrinsic Mode Functions (IMF) and they represent a sequence of frequencies from high-frequency through to a low-frequency, long-term trend. EEMD is an extension of Empirical Mode Decomposition (EMD) (Huang and Wu, 2008), which is calculated from only one decomposition of a time series. EMD often suffers from "mode mixing", where a given IMF contains a range of frequencies, and the EEMD method was developed as a way of reducing this effect. This is achieved by adding white noise to the data series, and conducting the EMD on this new series. This process is repeated a large number of times, with the arithmetic mean taken across the resulting set of trials. In this analysis, 1000 trials were conducted and white noise with a strength of 0.2 times the standard deviation of the time series was used after Qian et al. (2009).

A subjective decision needs to be made when using EEMD as to which IMFs represent the frequency of interest. The sum of the seventh through to the final IMF (which is set to 12) are taken to represent the annual cycle and longer timescale component (ALC) of temperature. This follows the general method of Qian et al. (2009). However, their analysis took the sum of the first six IMFs as the ALC, and hence our ALC is slightly smoother than their definition; this further reduces the possibility of multiple crossings of the 5°C threshold in the spring and autumn periods by the ALC. The higher-frequency variability represented by the first six components are taken to represent the supra-annual cycle variability, including synoptic-scale variability, that we wish to remove from the time series. It should be noted that the annual cycle definition used here is different to the Modulated Annual Cycle (MAC) that has been used in several previous analyses (Wu et al., 2008; Qian et al., 2011a,b; Qian and Zhang, 2015; Cornes et al., 2017), as the MAC removes the long-term trend from the series. In the annual cycle calculations used here the long-term trend is retained.

Since the EEMD requires a complete data sequence, missing values in the time series were filled using a cubic spline interpolation, up to a maximum span of 10 days. This infilling is done over the temporal dimension and the length of 10 days was chosen as we are interested in this analysis in removing synoptic-scale noise from the time series and retaining the lower frequency variability. As a consequence however, any series with a consecutive span of missing days longer then 10 days could not be processed using this method.

The GSL calculated using EEMD (GSL_{eemd}) is defined as the number of days between the first and last crossing of the 5°C threshold by the ALC in a given calendar year. This threshold is commonly used in GSL calculations (Qian et al., 2011b), including the ETCCDI definition. As with the index of the GSL defined by the ETCCDI, in years where the annual cycle remains above the threshold on the 1st January, then the start of the GSL is set to one. Similarly, where the annual cycle remains above the threshold at the end of the year, then the end of the season is set to the number of days in the year (N_{yr}). In this analysis the 29th February values have been removed to ensure a consistent number of days per year in the EEMD analysis, and hence $N_{yr} = 365$. See Cornes et al. (2018) for the underlying GSL data.

3 Trends and Variability in the GSL

Trends in the GSL indices were calculated using the Theil-Sen estimator. This is derived as the median of the slopes through all pairs of lines of the data points and is therefore less sensitive to outliers in a data series than least-squares regression. The statistical significance of the trends was calculated using the pre-whitening method described by Zhang et al. (2000); Wang and Swail (2001), which takes into account lag-1 autocorrelation in the significance estimates.

3.1 The long temperature series

Long-term trends in the GSL calculated from the three multi-century time series all display a strong positive trend over the last ∼200 years, of between 1 and 2 days decade^{-1} (see Tables S1, S2 and S3, *Suppl. Info.*). As has been previously noted, a higher rate of change occurred in the GS parameters over the last 30 years (Linderholm, 2006). This is also observed in these results, with the most striking example occurring in the St Petersburg series where a trend of 4 days decade^{-1} (95% CI [1.9–5.9]) occurred in the GSL_{eemd} series over the period 1960–2013 compared to 1.3 days decade^{-1} (95% CI [1.0–1.6]) over the period 1805–2013. This disparity arises because of a number of anomalously short growing seasons occurring during the 1960–70s (see Section 3.1 and Table S5 *Suppl. Info.*). The trends over the 1805–2015 period in the CET and Stockholm series are predominately due to earlier starts of the GS, in accordance with the findings of Prior and Perry (2014); for St. Petersburg the trends in the start and end of the GS calculated using the EEMD method are comparable.

The trends in the GSL_{eemd} and GSL_{etccdi} indices are practically indistinguishable in the St Petersburg and Stockholm series (Table S2, *Suppl. Info.*). A larger difference is evident in the CET series, with a trend over the 1772–2016 period of 1.9 days decade^{-1} (95% CI [1.1–2.7]) evident in the GSL_{eemd} index compared to 1.6 days decade^{-1} (95% CI [1.0-2.2]) in GSL_{etccdi} (Figure 2 and Table S1). This difference occurs as a result of a larger trend in the *end* of the GS in the GSL_{eemd} index; there is not a significant difference in the *start* of the GS. Nonetheless, as with the other two temperature series the difference in GSL trends from the two indices is not significant in the CET series. Significance in these trend-differences was determined by calculating the trend in the difference series (GSL_{etccdi} *minus* GSL_{eemd}) after Santer et al. (2000) (see Tables S1 and S2, *Suppl. Info.*).

Despite the trends not being significantly different in the two indices, values of the GSL for individual years can be substantially different in the three temperature series analysed here. This is particularly the case in the CET series, as is apparent from Figures 1 and 2. The year 2013 had the third largest difference in GSL values, and was 94 days shorter in the GSL_{eemd} index. The largest difference occurred in the year 1785 (104 days shorter in GSL_{eemd}), with the second largest difference occurring in 1855 (101 days shorter, see Table S4 *Suppl. Info.*). Both of these years were analogous to 2013 in that an exceptionally cold and dry spring season was preceded by a short mild spell in January (Kington, 2010). Differences in the decadal averages calculated from the two indices can also be large (see Table S5 *Suppl. Info.*).

Since the higher-frequency variance is removed from the temperature data in the EEMD-derived GS parameters, the relationship to seasonal mean temperatures is also much higher in these data. For example, the regression coefficient between the start of the GS and the mean December to March temperature is $r^2 = 0.28$ for the ETCCDI-derived parameters, compared to $r^2 = 0.61$ for the EEMD series (Table S7, *Suppl. Info.*). As a further reflection of the closer association to the low-frequency seasonal cycle, the start of the GS estimated using the EEMD method has a much stronger relationship (r^2=0.28) to the Oak bud-burst dates in the Robert Marsham series from Norfolk 1772–1958 (Thompson and Clark, 2008) compared to the ETCCDI method (r^2=0.05).

3.2 Trends across Europe

On average the thermal GS has lengthened at a rate of around 5 days decade^{-1} since 1965 across Europe (Figure 3). The average in trends calculated from either the GSL_{etccdi} or GSL_{eemd} index is very similar, and is in accordance with the findings of Menzel et al. (2003). That study used a version of the GSL_{etccdi} index to calculate the GSL and their results indicated considerable station-to-station variability in the trends. A much more coherent picture emerges from the results here using the GSL_{eemd} index. Most of the trends (80%,

n=645) across central and northern Europe in GSL_{eemd} are significant at $p<0.05$. In contrast only 29% are significant at that level in the GSL_{etccdi} index. This occurs as a result of a lower degree of interannual variability in the GSL_{eemd} index at most stations, as a consequence of the filtering-out of variability beyond the annual cycle. This variance-difference can also be seen in the results from the multi-centenary series, but only for the Stockholm and St. Petersburg series; in the CET the series the interannual variance in the parameters is slightly higher in the EEMD-derived parameters (Table S6 *Suppl. Info.*). This is likely a reflection of the CET being a regional average of temperature, as opposed to a point-value as is the case in the other series.

4 The Response of the GSL to Large-Scale Dynamics

Several previous studies have related the GSL, and the related frost-free period or spring onset, to atmospheric circulation at both the hemispheric and regional scales (Jones et al., 2002; Qian et al., 2009; Wypych et al., 2017; Strong and McCabe, 2017). Such studies are particularly important as any attempt to forecast the GSL is dependent on understanding the linkages with large-scale, low-frequency, atmosphere-ocean forcing mechanisms. However, Jones et al. (2002) achieved very poor correlations between an index representative of zonal flow across northwest Europe and growing season lengths calculated from four long daily temperature series from across Europe. In the GSL_{etccdi} index calculated from the CET series we also find no significant correlation to the winter NAO index of Jones et al. (1997). Conversely, the relationship with the GSL_{eemd} index is relatively strong ($r^2=0.23$, $p<0.001$ two-tailed test, calculated over the period 1821–2007). Similar results ($r^2=0.26$) are found when using the Paris-London westerly index (Cornes et al., 2013), which provides a localized measure of zonal flow across northwest Europe. The relationship of the GS to the NAO is attributable to the strong relationship of the NAO to the start of the GS (r^2=0.36) since there is no correlation to the end of growing season. This is the case even if the NAO values for the autumn season (SON) are used.

To further investigate the relationship of the GS parameters to large-scale atmospheric forcing, we have performed a Principal Component Analysis (PCA) using de-trended and standardized values of the start and end of the GS calculated from the ECA&D data (see Section 2.1) over the period 1965–2016. Stations are only used where the variance in the GS parameters is greater than zero over the 1965–2016 period. The PC time series have been regressed against the 500hPa geopotential height anomalies (relative to the 1961–1990 period) from the NCEP/NCAR reanalysis dataset (Kanamitsu et al., 2002) and sea-surface temperature anomalies from the COBE2-SST dataset (Hirahara et al., 2014). The start of the GS values are related to the prior winter (DJF) ocean-atmosphere conditions, while the concurrent autumn season (SON) mean anomalies are used for the end of the GS.

4.1 The start of the growing season

The first two components of the PCA applied to the start of the GS calculated using the EEMD method collectively explain around 57% of the interannual variability (Figure 4). Similar results are achieved when the start of the GS is calculated using the ETCCDI method (Figure S3, *Suppl. Info.*). However, in that case the results are less coherent and the first two components only explain 34.7% of the variance.

PC1 represents a zonal mode of variability, and in a positive phase is associated with an advance in the start of the GS (negative anomalies) across most of Europe but particularly so across central/northeastern regions. The slope coefficient of the regression of the PC time series against 500hPa geopotential heights (Figure 4 a) indicates that this component is associated with an NAO-type pattern of atmospheric circulation, with a clear annular shape across the Northern Hemisphere indicating a connection to the Northern Annular Mode. However, in contrast to the canonical NAO pattern (e.g. Barnston and Livezey, 1987) the southern node is situated eastward of its more usual position. This appears to reflect the mobility in the nodes of the NAO across the North Atlantic region that has been described in several previous studies (Cassou et al., 2004; Moore et al., 2013). These studies have indicated that an asynchronous pattern exists between different states of the NAO, with the southern node situated over the Iberian peninsula during positive phases, and in a more westerly position during negative phases. The concurrent (DJF) SST anomalies for this mode (Figure 4 b) display an expected NAO tripole relationship across the Atlantic region. The strongest relationship, however, is with SST anomalies across the North Sea and southern Baltic coasts. To some extent this may reflect the uneven sampling across Europe in this selection of stations, with the highest density being across Germany and Sweden. The PC time series (Figure 4 c) indicates no long-term trend in the occurrence of this pattern.

PC2 displays a distinct zonal pattern of PC loadings. In a positive phase this component represents earlier GS starting dates across Scandinavia and later dates across the rest of Europe (Figure 4 e), and is related to an anticyclonic ridge in the eastern Atlantic. This pattern is related to the second most dominant mode of atmospheric variability across the Atlantic region, the East-Atlantic pattern (Cassou et al., 2004), and is strongly associated with positive SST anomalies across the central Atlantic but especially across the Norwegian Sea (Figure 4 e). A clustering of strong negative phases of this pattern occurred in the late 1990s. This was preceded in the mid 1980s by a high frequency of strong positive states of the East-Atlantic pattern (Figure 4 f).

4.2 The end of the growing season

The first two components of the PCA for the end of the GS collectively explain 55% of the variation in the data (Figure 5). As with the start of the GS, similar results are achieved using the ETCCDI method of calculating the end of the GS (Figure S4, *Suppl. Info.*). Again, however, a less coherent picture emerges from these data, with the first two components collectively only explaining 35.2% of the variance.

In a positive mode PC1 represents a later end to the growing season (positive loadings) particularly across central and northern regions of Europe, whereas PC2 represents a split across the domain with advancement (retardation) across Scandinavia (central Europe). Both of these PCs are connected to an atmospheric circulation configuration reminiscent of the East-Atlantic/West Russia (Eurasia-type 2) teleconnection pattern (Barnston and Livezey, 1987). Relative to PC1, the North Atlantic and Russian nodes are stronger and more elongated in PC2, and the sub-polar node is weaker and more confined. This difference appears to have a profound effect on the pattern of the end of the GS anomalies.

The time series for PC1 indicates two strong positive occurrences of this component. The year 2006 experienced the highest PC loadings, and conditions during the Autumn season were extraordinarily warm across most areas of Europe (van Oldenborgh, 2007). A similarly strong example of this pattern occurred in Autumn 2000 (Blackburn and Hoskins, 2001).

In their analysis of variations in the frost-free period across the conterminous United States, Strong and McCabe (2017) highlighted the prominent influence of the Pacific-North America pattern on the GS start/end dates; their results reveal a weak association with the NAO. While direct comparison against their results is hindered by very different methods of analysis, the results in this section indicate that it is the Atlantic-centred NAO and East-Atlantic patterns that have the most influence on the interannual variance of the GS parameters across Europe, regardless of the GSL index used. Of note in this analysis is the distinction between zonal(meridional) patterns that affect the start(end) of the GS.

5 Conclusions

We have compared long-term trends and interannual variability across Europe in two indices of the GSL: the widely used ETCCDI definition and an alternative definition using the EEMD time-series decomposition method. Despite substantial differences in GS lengths for individual years, the long-term trends in the GSL across Europe are broadly similar in the two indices, and show an advancement of around 5 days decade^{-1} over the last 50 years. However, a much more coherent pattern of significant trends are found in the EEMD index as a result of the removal of the high-frequency, synoptic-scale variability. Furthermore, since the EEMD index captures the seasonal-cycle of temperature, it's connection to seasonal-mean hemispheric-scale atmospheric forcing mechanisms is more clearly defined. Around 57% of the interannual variability in the start GS can be explained by the NAO-type and East-Atlantic-type modes of atmospheric circulation variability during the winter season. Similarly around 55% of the variation in the end of the GS can be explained by East Atlantic/West Russia-type patterns during the autumn. Although we use the EEMD method in this analysis, other low-frequency filters, such as those reviewed by Deng and Fu (2018), could likely produce similar results. The key feature is that the synoptic-scale variability is removed from the GSL calculation, and the annual cycle and longer-term variability is retained.

In many phenological applications knowledge about the occurrence of synoptic-scale events, such as frost, are critical and metrics such as the Spring Indices (Schwartz et al., 2006, 2013) that are able to capture such events — and which are calibrated against phenological data — are key indicators. However, in climate monitoring applications a temperature-based index is required that captures the length of the GS and which broadly applies to a range of species and at a variety of locations; this would appear to be best achieved through the quantification of the low-frequency seasonal cycle of temperature by an index such as the EEMD metric. Further analyses are required to determine the relationship of this index to phenological data. However, a simple test carried out in this paper suggests that the start of the GS derived from the EEMD index has a closer relationship with the budburst dates in an Oak series at one site in England compared to the ETCCDI-related index. Further analyses are required to see if this is the case for other species and at different locations.

Acknowledgements

We acknowledge the data providers in the ECA&D project (Klein Tank et al., 2002). The station data and metadata are available at `http://www.ecad.eu`, and the GSL data are availabe from Cornes et al. (2018).

References

Barnston, A. G. and Livezey, R. E. (1987). Classification, seasonality and persistence of low frequency atmospheric circulation patterns.

Benjamini, Y. and Hochberg, Y. (1995). Controlling the False Discovery Rate: A Practical and Powerful Approach to Multiple Testing. *J. R. Stat. Soc. Ser. B*, 57(1):289–300.

Blackburn, M. and Hoskins, B. J. (2001). Atmospheric Variability and Extreme Autumn Rainfall in the UK. Technical report.

Cassou, C., Terray, L., Hurrell, J. W., and Deser, C. (2004). North Atlantic Winter Climate Regimes: Spatial Asymmetry, Stationarity with Time, and Oceanic Forcing. *J. Clim.*, 17(5):1055–1068, doi:10.1175/1520-0442(2004)017<1055:NAWCRS>2.0.CO;2.

Cornes, R., van der Schrier, G., and Squintu, A. (2018). Station-based Growing Season Length values across Europe calculated using EEMD and ETCCDI methods. Figshare repository, doi:10.6084/m9.figshare.6936227.

Cornes, R. C., Jones, P. D., Briffa, K. R., and Osborn, T. J. (2013). Estimates of the North Atlantic Oscillation back to 1692 using a Paris-London westerly index. *Int. J. Climatol.*, 33(1):228–248, doi:10.1002/joc.3416.

Cornes, R. C., Jones, P. D., and Qian, C. (2017). Twentieth-Century Trends in the Annual Cycle of Temperature across the Northern Hemisphere. *J. Clim.*, 30(15):5755–5773, doi:10.1175/JCLI-D-16-0315.1.

Davis, N. E. (1972). The variability of the onset of spring in Britain. *Q. J. R. Meteorol. Soc.*, 98(418):763–777, doi:10.1002/qj.49709841805.

Deng, Q. and Fu, Z. (2018). Comparison of methods for extracting annual cycle with changing amplitude in climate series. *Clim. Dyn.*, In press:1–12, doi:10.1007/s00382-018-4432-8.

Eden, P. (2013). March 2013, Coldest March since 1962; dullest since 1984 in East Anglia and the Southeast. *Weather*, 68(5):i–iv, doi:10.1002/wea.2013.

Hirahara, S., Ishii, M., and Fukuda, Y. (2014). Centennial-Scale Sea Surface Temperature Analysis and Its Uncertainty. *J. Clim.*, 27(1):57–75, doi:10.1175/JCLI-D-12-00837.1.

Huang, N. E. and Wu, Z. (2008). A review on Hilbert-Huang transform: Method and its applications to geophysical studies. *Rev. Geophys.*, 46(2), doi:10.1029/2007rg000228.

Jones, P. D., Briffa, K. R., Osborn, T. J., Moberg, A., and Bergström, H. (2002). Relationships between circulation strength and the variability of growing-season and cold-season climate in northern and central Europe. *The Holocene*, 12(6):643–656, doi:10.1191/0959683602hl577rp.

Jones, P. D., Jonsson, T., and Wheeler, D. (1997). Extension to the North Atlantic oscillation using early instrumental pressure observations from Gibraltar and south-west Iceland. *Int. J. Climatol.*, 17(13):1433–1450, doi:10.1002/(SICI)1097-0088(19971115)17:13<1433::AID-JOC203>3.0.CO;2-P.

Jones, P. D. and Lister, D. H. (2002). The Daily Temperature Record for St. Petersburg (1743–1996). *Clim. Change*, 53(1-3):253–267, doi:10.1023/A:101491880.

Kanamitsu, M., Ebisuzaki, W., Woollen, J., Yang, S.-K., Hnilo, J. J., Fiorino, M., and Potter, G. L. (2002). NCEP–DOE AMIP-II Reanalysis (R-2). *Bull. Am. Meteorol. Soc.*, 83(11):1631–1643.

Kington, J. (2010). *Collins New Naturalist Library: British Climate and Weather.* HarperCollins UK.

Klein Tank, A. M. G., Wijngaard, J. B., Können, G. P., Böhm, R., Demarée, G., Gocheva, A., Mileta, M., Pashiardis, S., Hejkrlik, L., Kern-Hansen, C., Heino, R., Bessemoulin, P., Müller-Westermeier, G., Tzanakou, M., Szalai, S., Pálsdóttir, T., Fitzgerald, D., Rubin, S., Capaldo, M., Maugeri, M., Leitass, A., Bukantis, A., Aberfeld, R., van Engelen, A. F. V., Forland, E., Mietus, M., Coelho, F., Mares, C., Razuvaev, V., Nieplova, E., Cegnar, T., Antonio López, J., Dahlström, B., Moberg, A., Kirchhofer, W., Ceylan, A., Pachaliuk, O., Alexander, L. V., and Petrovic, P. (2002). Daily dataset of 20th-century surface air temperature and precipitation series for the European Climate Assessment. *Int. J. Climatol.*, 22(12):1441–1453.

Klok, E. J. and Klein Tank, A. M. G. (2009). Updated and extended European dataset of daily climate observations. *Int. J. Climatol.*, 29(8):1182–1191.

Kunkel, K. E., Easterling, D. R., Hubbard, K., and Redmond, K. (2004). Temporal variations in frost-free season in the United States: 1895–2000. *Geophys. Res. Lett.*, 31(3):L03201, doi:10.1029/2003GL018624.

Linderholm, H. W. (2006). Growing season changes in the last century. *Agric. For. Meteorol.*, 137(1-2):1–14, doi:10.1016/j.agrformet.2006.03.006.

Menzel, A., Jakobi, G., Ahas, R., Scheifinger, H., and Estrella, N. (2003). Variations of the climatological growing season (1951-2000) in Germany compared with other countries. *Int. J. Climatol.*, 23(7):793–812, doi:10.1002/joc.915.

Moberg, A., Bergström, H., Krigsman, J. R., and Svanered, O. (2002). Daily air temperature and pressure series for {S}tockholm (1756–1998). *Clim. Change*, 54:249–250.

Moore, G. W. K., Renfrew, I. A., and Pickart, R. S. (2013). Multidecadal Mobility of the North Atlantic Oscillation. *J. Clim.*, 26(8):2453–2466, doi:10.1175/JCLI-D-12-00023.1.

Parker, D. E., Legg, T. P., and Folland, C. K. (1992). A new daily central {E}ngland temperature series, 1772–1991. *Int. J. Climatol.*, 12:317–342.

Prior, M. J. and Perry, M. C. (2014). Analyses of trends in air temperature in the United Kingdom using gridded data series from 1910 to 2011. *Int. J. Climatol.*, 34(14):3766–3779, doi:10.1002/joc.3944.

Qian, C., Fu, C., and Wu, Z. (2011a). Changes in the Amplitude of the Temperature Annual Cycle in China and Their Implication for Climate Change Research. *J. Clim.*, 24(20):5292–5302, doi:10.1175/jcli-d-11-00006.1.

Qian, C., Fu, C., Wu, Z., and Yan, Z. (2009). On the secular change of spring onset at Stockholm. *Geophys. Res. Lett.*, 36(12):n/a—-n/a, doi:10.1029/2009GL038617.

Qian, C., Fu, C., Wu, Z., and Yan, Z. (2011b). The role of changes in the annual cycle in earlier onset of climatic spring in northern China. *Adv. Atmos. Sci.*, 28(2):284–296, doi:10.1007/s00376-010-9221-1.

Qian, C. and Zhang, X. (2015). Human influences on changes in the temperature seasonality in mid- to high-latitude land areas. *J. Clim.*, 28(15):5908–5921, doi:10.1175/JCLI-D-14-00821.1.

Robeson, S. M. (2002). Increasing Growing-Season Length in Illinois During the 20th Century. *Clim. Change*, 52:219–238, doi:10.1023/A:1013088011223.

Santer, B. D., Wigley, T. M. L., Boyle, J. S., Gaffen, D. J., Hnilo, J. J., Nychka, D., Parker, D. E., and Taylor, K. E. (2000). Statistical significance of trends and trend differences in layer-average atmospheric temperature time series. *J. Geophys. Res. Atmos.*, 105(D6):7337–7356.

Schwartz, M. D., Ahas, R., and Aasa, A. (2006). Onset of spring starting earlier across the Northern Hemisphere. *Glob. Chang. Biol.*, 12(2):343–351, doi:10.1111/j.1365-2486.2005.01097.x.

Schwartz, M. D., Ault, T. R., and Betancourt, J. L. (2013). Spring onset variations and trends in the continental United States: past and regional assessment using temperature-based indices. *Int. J. Climatol.*, 33(13):2917–2922, doi:10.1002/joc.3625.

Squintu, A. A., van der Schrier, G., Brugnara, Y., and Klein Tank, A. (2018). Homogenization of daily ECA&D temperature series. *Int. J. Climatol.*, in press, doi:10.1002/joc.5874.

Strong, C. and McCabe, G. J. (2017). Observed variations in U.S. frost timing linked to atmospheric circulation patterns. *Nat. Commun.*, 8:15307, doi:10.1038/ncomms15307.

Thompson, R. and Clark, R. M. (2008). Is spring starting earlier? *The Holocene*, 181:95–104, doi:10.1177/0959683607085599.

van Oldenborgh, G. J. (2007). How unusual was autumn 2006 in Europe? *Clim. Past*, 3(4):659–668, doi:10.5194/cp-3-659-2007.

Walther, A. and Linderholm, H. W. (2006). A comparison of growing season indices for the Greater Baltic Area. *Int. J. Biometeorol.*, 51(2):107–118, doi:10.1007/s00484-006-0048-5.

Wang, X. L. and Swail, V. R. (2001). Changes of Extreme Wave Heights in Northern Hemisphere Oceans and Related Atmospheric Circulation Regimes. *J. Clim.*, 14(10):2204–2221.

Wu, Z. and Huang, N. E. (2009). Ensemble Empirical Mode Decomposition: a Noise-Assisted Data Analysis Method. *Adv. Adapt. Data Anal.*, 01(01):1–41, doi:10.1142/S1793536909000047.

Wu, Z., Schneider, E. K., Kirtman, B. P., Sarachik, E. S., Huang, N. E., and Tucker, C. J. (2008). The modulated annual cycle: an alternative reference frame for climate anomalies. *Clim. Dyn.*, 31(7-8):823–841, doi:10.1007/s00382-008-0437-z.

Wypych, A., Ustrnul, Z., Sulikowska, A., Chmielewski, F. M., and Bochenek, B. (2017). Spatial and temporal variability of the frost-free season in Central Europe and its circulation background. *Int. J. Climatol.*, 37(8):3340–3352, doi:10.1002/joc.4920.

Yu, L., Zhong, S., Bian, X., Heilman, W. E., and Andresen, J. A. (2014). Temporal and spatial variability of frost-free seasons in the Great Lakes region of the United States. *Int. J. Climatol.*, 34(13):3499–3514, doi:10.1002/joc.3923.

Zhang, X., Alexander, L., Hegerl, G. C., Jones, P., Tank, A. K., Peterson, T. C., Trewin, B., and Zwiers, F. W. (2011). Indices for monitoring changes in extremes based on daily temperature and precipitation data. *Wiley Interdiscip. Rev. Clim. Chang.*, 2(6):851–870.

Zhang, X., Vincent, L. a., Hogg, W. D., and Niitsoo, A. (2000). Temperature and precipitation trends in Canada during the 20th century. *Atmosphere-Ocean*, 38(3):395–429, doi:10.1080/07055900.2000.9649654.

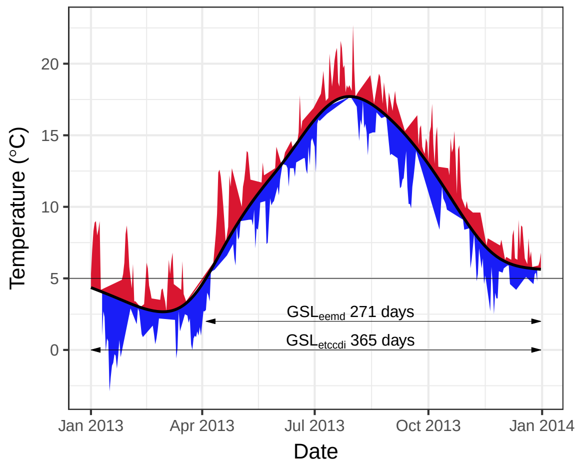

Figure 1: The daily mean Central England Temperature series for the year 2013. The black line marks the annual cycle extracted using EEMD, with the colouring indicating daily values above or below this line. The duration of the GSL using the two different methods are indicated.

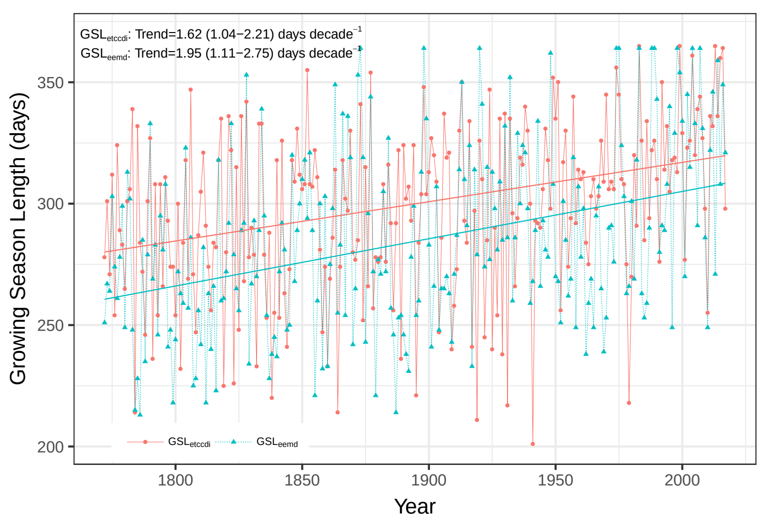

Figure 2: Trends in the $\mathrm{GSL}_{\mathrm{eemd}}$ and $\mathrm{GSL}_{\mathrm{etccdi}}$ indices calculated from the CET daily mean temperature series 1772–2017. The trend and 95% confidence intervals are indicated.

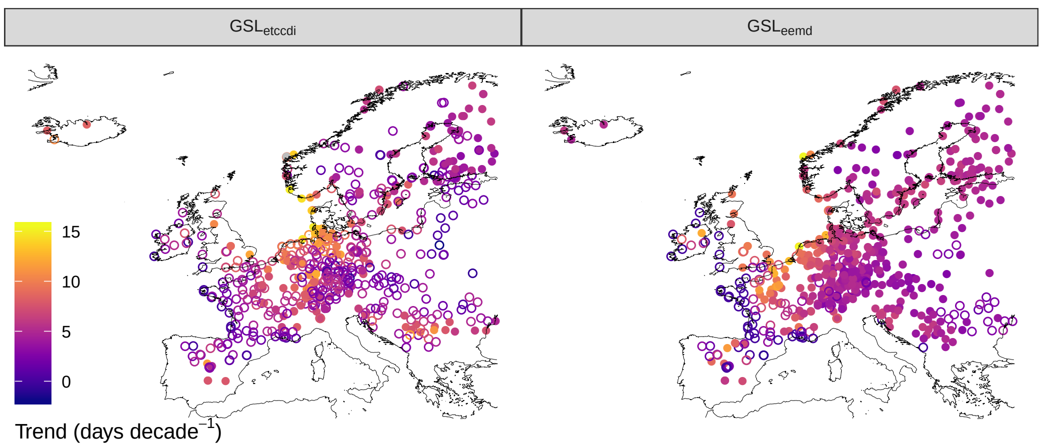

Figure 3: Trends in the station series across Europe (1965–2016). Open circles indicate trends that are not significant at p<0.05 (two-tailed test), after adjustment of the p-values to account for false detection following Benjamini and Hochberg (1995). Stations are excluded where the GSL=365 for all years. Outliers (trends>=18 days decade^{-1}) are coloured grey (one value).

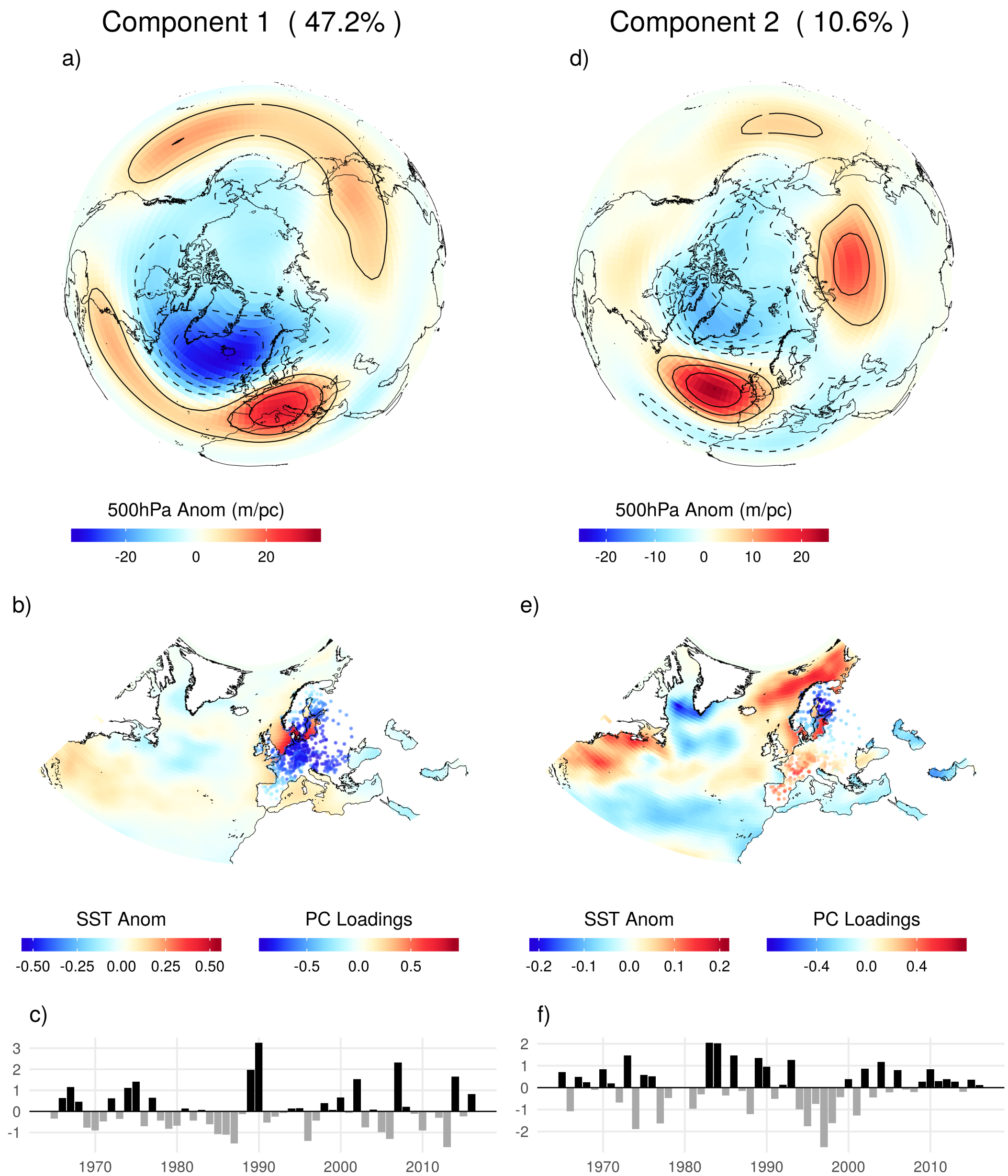

Figure 4: The teleconnection patterns associated with the first two Principal Components (PC) of the start of the growing season. In a) and d) the slope coefficient from the regression of the respective PC time time series against winter average (DJF) 500hPa geopotential height anomalies are plotted. In b) and e) a similar slope coefficient is calculated using SST anomalies. In those figures the PC loadings at each of the European stations are also indicated. In c) and f) the PC time series (in standardized units) are plotted.

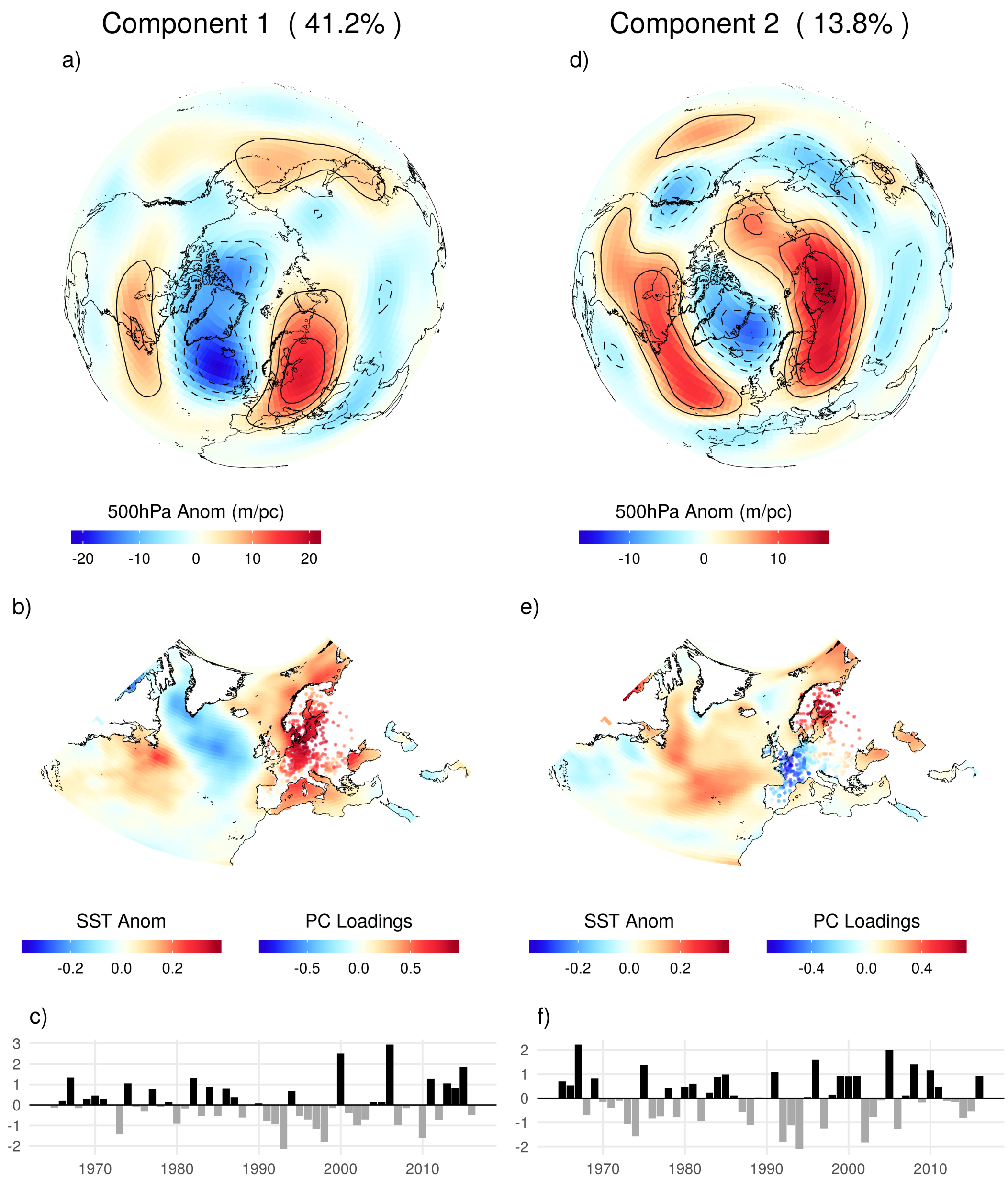

Figure 5: As Figure 4 but for the end of the growing season and using 500hPa height/SST anomalies from the autumn season (SON).